

# Operation Modes of the Planar 3-RRR Manipulator

Aravind Baskar and Sandipan Bandyopadhyay<sup>(✉)</sup>

Department of Engineering Design, Indian Institute of Technology Madras,  
Chennai 600036, India

krishna.arvind91@gmail.com, sandipan@iitm.ac.in

**Abstract.** The planar 3-RRR parallel manipulator is known to have six assembly modes. However, analysing it in the framework of spatial kinematics reveals that it has a total of twelve assembly modes, six in each of the two possible operation modes. The modes are derived using a Study parameter formulation first, and later confirmed in another formulation in the joint-space, and finally visualised in terms of the planar constraint curves generated by the sub-chains of the manipulator. Numerical results show that all the twelve modes can be real for certain inputs.

**Keywords:** Operation modes · Study's kinematic mapping · Discrete Screw Axis (DSA) · Forward Kinematic Univariate (FKU)

## 1 Introduction

The planar 3-RRR manipulator has six assembly modes, as mentioned in many existing reports, e.g., Gosselin *et al.* [1]. However, if the forward kinematic analysis of this manipulator is performed in the joint space, it shows twelve assembly modes. In this work, this problem is investigated from multiple perspectives, namely: the kinematic mapping of Study; the constraints in the joint space; and the constraints generated by the sub-chains of the manipulator. This work is similar to the study of the 3-RPR manipulator by Husty [3], using the Study parameter representation of  $\mathbb{SE}(2)$ . However, in the current work, the full spatial setup is used in the kinematic modelling, as in [4], which leads to results that are strikingly similar. On the other hand, this work is also motivated by [6], where the kinematic analysis is performed on the basis of the constraint equations in the joint-space of the 3-RPS. Analogous results are obtained in this case as well, and nice inferences can be drawn based on these to present a consistent interpretation of the results obtained from various approaches. The main results are that the manipulator has six assembly modes in each of the two of its operation modes, though only one mode is apparent at a time, as unlike in the 3-RPS, a transition between the modes is not (physically) possible in this case. It is (mathematically) possible for all the assembly modes to be real at the same time, as shown with the help of a numerical example. Also, the solutions can

be explained geometrically in terms of the intersections of the constraint curves generated by the sub-chains of the manipulator.

The rest of the paper is presented as follows: Sect. 2 describes the forward kinematic analysis of the problem in the task space while Sect. 3 discusses the same problem in the joint space. Section 4 concludes the paper.

## 2 Forward Kinematic Analysis Using Study Parameters

The forward kinematic problems of planar 3-degrees-of-freedom parallel manipulators have been studied using the planar kinematic mapping (see, e.g., [3] in case of 3-RPR manipulator). In the following, spatial kinematic mapping is used to study the planar 3-RRR manipulator, leading to certain new and interesting observations.

### 2.1 Kinematic Model

The manipulator is shown in Fig. 1. The fixed base  $b_1b_2b_3$  and the moving platform  $p_1p_2p_3$  are both equilateral triangles, of side lengths  $b$  and  $a$  respectively. Three limbs of R-R-R architecture, each having an actuated link of length  $l$  and a passive link of length  $r$ , connect the two platforms. The active joint angles are given by  $\theta = [\theta_1, \theta_2, \theta_3]^T$ , and the passive joint angles by  $\phi = [\phi_1, \phi_2, \phi_3]^T$ . The frame  $\{A\}$ , given by  $O_A-X_A Y_A Z_A$ , serves as the global frame of reference. Likewise, frame  $\{B\}$ , attached to the moving platform, denotes the moving frame. The vertices of the two platforms are expressed in projective coordinates:  ${}^B p_1 = [0, 0, 0, 1]^T$ ,  ${}^B p_2 = [a, 0, 0, 1]^T$ ,  ${}^B p_3 = [\frac{a}{2}, \frac{\sqrt{3}a}{2}, 0, 1]^T$ , and

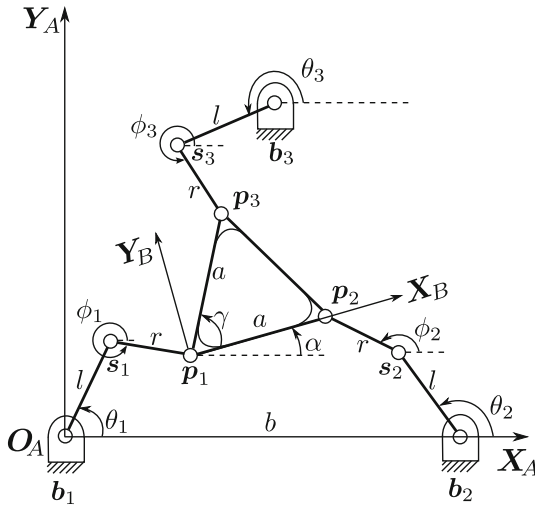


Fig. 1. Planar 3-RRR parallel manipulator

${}^A\mathbf{b}_1 = [0, 0, 0, 1]^\top$ ,  ${}^A\mathbf{b}_2 = [b, 0, 0, 1]^\top$ ,  ${}^A\mathbf{b}_3 = \left[ \frac{b}{2}, \frac{\sqrt{3}}{2}b, 0, 1 \right]^\top$ , where the fourth coordinate, 1, is the projective coordinate, and the leading superscripts  $A$  and  $B$  indicate the frame of reference. The frame  $\{B\}$  is related to  $\{A\}$  through a  $4 \times 4$  homogeneous transformation matrix,  ${}^A_B\mathbf{T}$ , expressed in terms of the *Study-parameters*. The Study parameters, namely,  $x_0 : x_1 : x_2 : x_3 : y_0 : y_1 : y_2 : y_3$ , represent spatial motions of a rigid-body via the *kinematic map*  $\kappa : \mathbb{P}^7 \rightarrow \mathbb{SE}(3)$ , when they satisfy the following constraints (see, e.g., [5]):

$$\text{Equation of the Study quadric: } x_0y_0 + x_1y_1 + x_2y_2 + x_3y_3 = 0, \quad (1)$$

$$\text{Normalisation constraint: } x_0^2 + x_1^2 + x_2^2 + x_3^2 = 1. \quad (2)$$

## 2.2 Kinematic Constraint Equations and the Operation Modes

The *loop-closure* constraints are derived from the fact that the passive links are rigid, and have a constant length  $r$  each:

$$\|{}^A\mathbf{p}_i - {}^A\mathbf{s}_i\|^2 - r^2 = 0, \quad i = 1, 2, 3, \quad (3)$$

where  ${}^A\mathbf{s}_i$  locate the tip of the active links, given by  ${}^A\mathbf{s}_1 = [l \cos \theta_1, l \sin \theta_1, 0, 1]^\top$ ,  ${}^A\mathbf{s}_2 = [b + l \cos \theta_2, l \sin \theta_2, 0, 1]^\top$ ,  ${}^A\mathbf{s}_3 = \left[ \frac{b}{2} + l \cos \theta_3, \frac{\sqrt{3}}{2}b + l \sin \theta_3, 0, 1 \right]^\top$ .

Equations (3) locate each of the points  $\mathbf{p}_i$  on a sphere centered at  $\mathbf{s}_i$ . To incorporate the planar nature of the manipulator, additional constraints are generated, by setting the  $Z$  component of  ${}^A\mathbf{p}_i - {}^A\mathbf{s}_i$  to zero, and manipulating them a little:

$$\eta_1 : x_3y_0 + x_2y_1 - x_1y_2 - x_0y_3 = 0, \quad (4)$$

$$\eta_2 : x_1x_3 - x_0x_2 = 0, \quad (5)$$

$$\eta_3 : x_0x_1 + x_2x_3 = 0. \quad (6)$$

The forward kinematic problem is represented by the set of Eqs. (1–6). An analysis of the planarity constraints (Eqs. (4–6)) along with the Study quadric equation (Eq. (1)) and the normalisation constraint (Eq. (2)) lead to two distinct *operation modes* (see [4] for a similar analysis of the 3-RPS manipulator):

- Mode 1, characterised by  $x_1 = x_2 = 0$ ,  $x_0^2 + x_3^2 \neq 0$ :  
 From Eqs. (1) and (4), one finds that  $y_0 = y_3 = 0$ , as the non-trivial solution leads to  $x_0^2 + x_3^2 = 0$ , which cannot be admitted. Thus, the variables  $x_1, x_2, y_0, y_3$  are eliminated from the equations in this mode, and the normalising constraint (in Eq. (2)) gets reduced to  $x_0^2 + x_3^2 = 1$ .
- Mode 2, characterised by  $x_0 = x_3 = 0$ ,  $x_1^2 + x_2^2 \neq 0$ :  
 Using a similar argument, it can be established that  $y_1 = y_2 = 0$  in this operation mode; the normalising constraint (Eq. (2)) becomes  $x_1^2 + x_2^2 = 1$ .

It may be noted that the two modes described above cover *all* the possible solutions of the forward kinematics problem. Furthermore, the two modes are *dis-joint*, as their intersection would lead to the *exceptional generator*, characterised by  $x_0 = x_1 = x_2 = x_3 = 0$ , which is physically inadmissible.

### 2.3 Derivation of the Forward Kinematic Univariate (FKU)

In the following, the loop-closure equations are reduced to a univariate polynomial equation (termed as the *Forward Kinematic Univariate (FKU)* [6]) following a sequence of elimination of variables. For the sake of brevity, only mode 1 is explained.

In mode 1, Eqs. (2 and 3) reduce to:

$$g_1 : l^2 - r^2 + 4l \sin \theta_1(x_0y_2 + x_3y_1) + 4l \cos \theta_1(x_0y_1 - x_3y_2) + 4(y_1^2 + y_2^2) = 0, \quad (7)$$

$$g_2 : (a - b)^2 + l^2 - r^2 + 2l \cos \theta_2(a(2x_3^2 - 1) + b + 2x_0y_1 - 2x_3y_2) + 4abx_3^2 - 4x_3y_2(a + b) + 4l \sin \theta_2(-ax_0x_3 + x_0y_2 + x_3y_1) - 4ax_0y_1 + 4bx_0y_1 + 4(y_1^2 + y_2^2) = 0, \quad (8)$$

$$g_3 : (a - b)^2 + l^2 - r^2 + l \sin \theta_3(a(\sqrt{3}(2x_3^2 - 1) - 2x_0x_3) + \sqrt{3}b + 4x_0y_2 + 4x_3y_1) + l \cos \theta_3(a(2x_3(\sqrt{3}x_0 + x_3) - 1) + b + 4x_0y_1 - 4x_3y_2) + 4abx_3^2 + 2x_3(a + b)(\sqrt{3}y_1 - y_2) - 2ax_0y_1 - 2\sqrt{3}ax_0y_2 + 2bx_0y_1 + 2\sqrt{3}bx_0y_2 + 4(y_1^2 + y_2^2) = 0, \quad (9)$$

$$g_4 : x_0^2 + x_3^2 - 1 = 0. \quad (10)$$

Therefore, mode 1 is represented by the ideal  $\langle g_1, g_2, g_3, g_4 \rangle$ . The steps to derive the FKU from this are:

1. Compute  $h_1 = g_2 - g_1$ , and  $h_2 = g_3 - g_1$ , which are linear in  $y_1, y_2$ .
2. Obtain  $y_1, y_2$  from  $h_1 = 0, h_2 = 0$ .
3. Substitute the values of  $y_1, y_2$  in  $g_1 = 0$ , to obtain the equation  $g'_1 = 0$  in  $x_0$  and  $x_3$ . The polynomial  $g'_1$  is of degree six in  $x_3$ .
4. Divide the polynomial  $g'_1$  by  $g_4$ , treating both as polynomials in  $x_3$ , and obtain an expression for  $x_3$  by solving the linear equation resulting from setting the remainder to zero.
5. Substitute  $x_3$  back in  $g_4$  to obtain the univariate in  $x_0$ .

The FKU is of degree 6 in  $x_0^2$ , hence there are a maximum of 6 real assembly modes, as each root is counted twice due to the nature of the kinematic map. A similar analysis leads to analogous results in mode 2.

### 2.4 Numerical Results and Interpretations

The above formulation is demonstrated via a numerical example, for the architecture parameters<sup>1</sup>  $l = 6/7, r = 13/14, a = 11/14$  and  $b = 1$ . The set of input joint angles given by  $\theta = [\pi/4, 5\pi/4, 3\pi/2]^T$  is found to produce 6 real solutions for each of the modes, which are listed in Table 1.

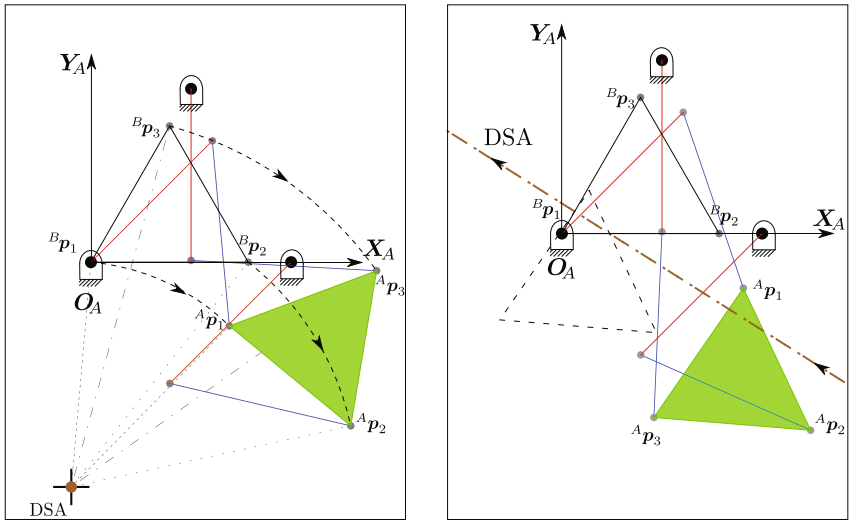
---

<sup>1</sup> All the linear dimensions are scaled by the base length,  $b$ , and are therefore unit-less; all angles are in radians.

**Table 1.** Twelve real solutions to forward kinematics

Operation mode	Assembly mode	$x_0$	$x_1$	$x_2$	$x_3$	$y_0$	$y_1$	$y_2$	$y_3$
Mode 1	1	-0.985	0	0	-0.172	0	-0.057	0.025	0
	2	-0.941	0	0	0.338	0	0.379	-0.033	0
	3	-0.852	0	0	0.523	0	-0.360	0.353	0
	4	-0.381	0	0	0.925	0	0.060	-0.011	0
	5	-0.350	0	0	-0.937	0	-0.058	-0.299	0
	6	-0.169	0	0	0.986	0	-0.116	0.795	0
Mode 2	1	0	-0.983	-0.185	0	-0.155	0	0	0.178
	2	0	-0.941	0.338	0	0.278	0	0	-0.335
	3	0	-0.845	0.535	0	-0.456	0	0	-0.127
	4	0	-0.369	0.930	0	0.028	0	0	-0.835
	5	0	-0.341	-0.940	0	-0.099	0	0	0.544
	6	0	-0.172	0.985	0	-0.133	0	0	-0.083

It is of interest to study the operation modes of the manipulator in terms of the finite screw motions generated by them. In mode 1, the motion is equivalent to a *pure* rotation about the *discrete screw axis (DSA)* [4], which is parallel to the  $Z$  axis and intersects the  $XY$  plane at  $x = y_2/x_3, y = -y_1/x_3$ . The pitch of the screw is null, as expected. Figure 2a shows the screw motion, using the numerics corresponding to assembly mode 2 of operation 1 from Table 1.



(a) Mode 1: The triangle  ${}^B p_1 {}^B p_2 {}^B p_3$  represented in local frame, when rotated about the DSA, transforms to the final position  ${}^A p_1 {}^A p_2 {}^A p_3$  (filled triangle), indicating a pure-rotation.

(b) Mode 2: The interim position (dashed) is reached through  $\pi$ -rotation about the DSA from the home position  ${}^B p_1 {}^B p_2 {}^B p_3$ . The final position  ${}^A p_1 {}^A p_2 {}^A p_3$  (filled) is then attained through translation along the DSA.

**Fig. 2.** Screw motion characteristics of the operation modes

The motion generated in mode 2 is not physically realisable without a disassembly of the manipulator, as it involves a rotation through  $\pi$  about a *horizontal* DSA. The equation of the DSA in the plane is found to be  $y = (x_2x + y_3)/x_1$ . Such screws have been termed as the  $\pi$ -screws in [4]. Figure 2b depicts the motion and the corresponding DSA for the assembly mode 3 of operation mode 2 listed in Table 1.

### 3 Forward Kinematic Analysis in the Joint Space

In this section, the forward kinematic analysis is performed in terms of the passive joint angles. Existence of the operation modes is brought out and the relationship between the two modes is established in terms of certain properties of the FKU.

#### 3.1 Derivation of the FKU and Its Interpretation

In this case, the end-points of the passive links are expressed in terms of the active and the passive joint angles as follows:  ${}^A\mathbf{p}_1 = {}^A\mathbf{s}_1 + [r \cos \phi_1, r \sin \phi_1, 0, 1]^T$ ,  ${}^A\mathbf{p}_2 = {}^A\mathbf{s}_2 + [r \cos \phi_2, r \sin \phi_2, 0, 1]^T$ ,  ${}^A\mathbf{p}_3 = {}^A\mathbf{s}_3 + [r \cos \phi_3, r \sin \phi_3, 0, 1]^T$ , where  ${}^A\mathbf{s}_i, i = 1, 2, 3$  are given in Sect. 2.2. Equating the distance between each distinct pair of vertices of the moving platform to the known value  $a$ , the loop-closure constraints are obtained as:

$$f_1(\phi_1, \phi_2) \triangleq ({}^A\mathbf{p}_1 - {}^A\mathbf{p}_2) \cdot ({}^A\mathbf{p}_1 - {}^A\mathbf{p}_2) - a^2 = 0, \tag{11}$$

$$f_2(\phi_2, \phi_3) \triangleq ({}^A\mathbf{p}_2 - {}^A\mathbf{p}_3) \cdot ({}^A\mathbf{p}_2 - {}^A\mathbf{p}_3) - 2a^2(1 - \cos \gamma) = 0, \tag{12}$$

$$f_3(\phi_1, \phi_3) \triangleq ({}^A\mathbf{p}_3 - {}^A\mathbf{p}_1) \cdot ({}^A\mathbf{p}_3 - {}^A\mathbf{p}_1) - a^2 = 0, \tag{13}$$

where  $\gamma = \pi/3$  is the interior angle of the triangular moving platform. The parameter  $\gamma$  is retained in its symbolic form to facilitate certain inferences drawn later in the paper. Equations (11–13) are linear in the sine and cosine of each of the passive angles, from which an FKU in  $t_2 = \tan(\phi_2/2)$  can be obtained easily following the elimination/transformation sequence depicted below<sup>2</sup>:

$$\left. \begin{array}{l} f_1(\phi_1, \phi_2) = 0 \\ f_3(\phi_1, \phi_3) = 0 \end{array} \right) \xrightarrow{\times \phi_1} \left. \begin{array}{l} u(\phi_2, \phi_3) = 0 \\ f_2(\phi_2, \phi_3) = 0 \end{array} \right) \begin{array}{l} \xrightarrow{\phi_3 \rightarrow t_3} v_1(t_3, \phi_2) = 0 \\ \xrightarrow{\phi_3 \rightarrow t_3} v_2(t_3, \phi_2) = 0 \end{array} \xrightarrow{\times t_3} w(\phi_2) = 0.$$

The notation ‘ $\xrightarrow{\times x}$ ’ denotes the elimination of the variable  $x$  from two algebraic equations preceding it, while ‘ $\xrightarrow{\phi_i \rightarrow t_i}$ ’ indicates the conversion of an equation in  $\phi_i$  to its polynomial equivalent in the variable  $t_i = \tan(\phi_i/2)$ . The equation  $w(\phi_2) = 0$ , when converted to a polynomial in  $t_2 = \tan(\phi_2/2)$ , is of degree 12,

<sup>2</sup> The derivation of this FKU is neither difficult, nor novel; hence the details are omitted for the sake of brevity.

indicating the possibility of existence of 12 real assembly modes—a result that matches with the previous analysis. The FKU decomposes into two factors as follows:

$$w(\gamma, t_2) = j_1(\gamma, t_2)j_2(\gamma, t_2), \text{ where } j_1(\gamma, t_2) = j_2(-\gamma, t_2). \quad (14)$$

Equation (14) confirms the relation between the two modes, as mode 2 corresponds to a moving platform that has been *flipped* up-side down, or equivalently, one in which the sequence of the vertices have been changed from CCW to CW. Also, it has been verified symbolically, that  $j_i(\gamma, t_2) = 0$  is the FKU for the mode  $i$ ,  $i = 1, 2$ .

### 3.2 Geometric Interpretation of the Operation Modes

It is well-known that the forward kinematics of certain planar three degrees-of-freedom parallel manipulators is equivalent to the problem of intersection of the *coupler curve* of a four-bar mechanism and a circle, which leads to a maximum of six assembly modes (see, e.g., [2]). In Fig. 3a, the dotted (blue) curve is the locus of  $p_3$  as a part of the four-bar sub-chain  $s_1p_1p_2s_1$ , with  $s_1s_2$  as its ground link, corresponding to mode 1 of operation, superimposed over the assembly mode shown in Fig. 2a. The circle represents the locus of  $p_3$  as a part of the sub-chain  $b_3s_3p_3$ , once the input  $\theta_3$  is given. The solid (red) curve in Fig. 3b corresponds to the mode 2, and is obtained by rotating the coupler link  $p_1p_2$  about the axis  $X_B$  by  $\pi$ -radians, and then performing a similar analysis. The solutions marked on Fig. 3b correspond to the numerics presented in Sect. 2.4. These figures can be thought of as a visual interpretation of Eq. (14).

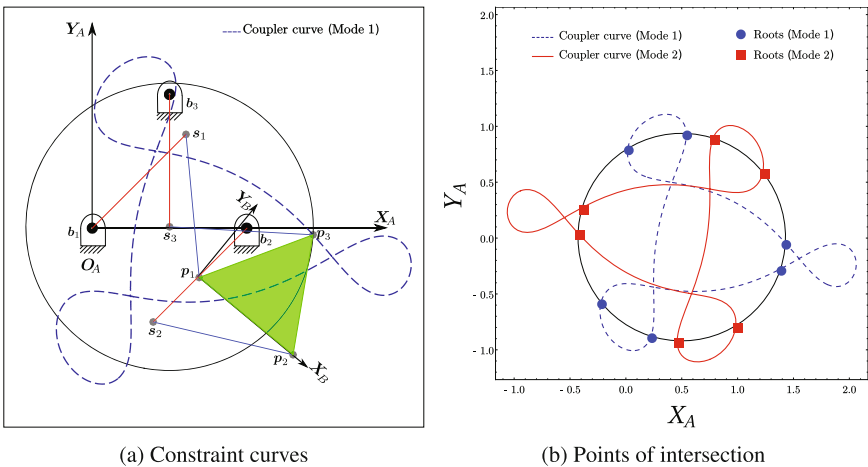


**Fig. 3.** Location of  $p_3$  as the intersection of the two planar curves. (Color figure online)

## 4 Conclusion

This paper analyses the planar 3-RRR manipulator, to establish its two operation modes, and the six assembly modes in each. This result is first derived using the Study parameters, and then corroborated with the results obtained from the study of the kinematics of the manipulator in its joint space. Finally, the results are unified using a graphical visualisation of the assembly modes, in terms of the intersection of the constraint curves generated by the sub-chains of the manipulator. It is shown, that mathematically all the twelve assembly modes can be real at the same time, though physically it is impossible for the manipulator to transit from one operation mode to the other, and hence only one operation mode is apparent any time.

## References

1. Gosselin, C., Sefrioui, J.: Polynomial solutions for the direct kinematic problem of planar three-degree-of-freedom parallel manipulators. In: *Robots in Unstructured Environments, 1991 ICAR, Fifth International Conference on Advanced Robotics*, pp. 1124–1129. IEEE (1991)
2. Hunt, K.: Structural kinematics of in-parallel-actuated robot-arms. *J. Mech. Transm. Autom. Des.* **105**(4), 705–712 (1983)
3. Husty, M.L.: Non-singular assembly mode change in 3-RPR-parallel manipulators. In: *Computational Kinematics*, pp. 51–60. Springer (2009)
4. Schadlbauer, J., Walter, D., Husty, M.: The 3-RPS parallel manipulator from an algebraic viewpoint. *Mechanism Mach. Theory* **75**, 161–176 (2014)
5. Selig, J.: *Geometric Fundamentals of Robotics*. Springer Science+Business Media Inc., Berlin (2005)
6. Srivatsan, R.A., Bandyopadhyay, S.: Analysis of constraint equations and their singularities. In: *Advances in Robot Kinematics*, pp. 429–436. Springer (2014)